ELSEVIER

Biochimica et Biophysica Acta 1458 (2000) 199–219

BIOCHIMICA ET BIOPHYSICA ACTA
BBA

www.elsevier.com/locate/bba

Proton and hydrogen currents in photosynthetic water oxidation

Cecilia Tommos [a], Gerald T. Babcock [b,*]

[a] *Johnson Research Foundation, Department of Biochemistry and Biophysics, University of Pennsylvania, Philadelphia, PA 19104, USA*
[b] *Department of Chemistry, Michigan State University, East Lansing, MI 48824, USA*

Received 1 April 1999; accepted 1 December 1999

Abstract

The photosynthetic processes that lead to water oxidation involve an evolution in time from photon dynamics to photochemically-driven electron transfer to coupled electron/proton chemistry. The redox-active tyrosine, Y_Z, is the component at which the proton currents necessary for water oxidation are switched on. The thermodynamic and kinetic implications of this function for Y_Z are discussed. These considerations also provide insight into the related roles of Y_Z in preserving the high photochemical quantum efficiency in Photosystem II (PSII) and of conserving the highly oxidizing conditions generated by the photochemistry in the PSII reaction center. The oxidation of Y_Z by P_{680}^+ can be described well by a treatment that invokes proton coupling within the context of non-adiabatic electron transfer. The reduction of $Y_Z^\bullet$, however, appears to proceed by an adiabatic process that may have hydrogen-atom transfer character.

Keywords: Photosystem II; Oxygen-evolving complex; Water-oxidizing complex; Oxygen evolution; Water oxidation; Tyrosine radical; Redox-active amino acid

1. Overview of Photosystem II (PSII) structure, energetics, and water oxidation

The oxidation of water to produce dioxygen occurs according to the half-cell reaction:

$$O_2 + 4H^+ + 4e^- \leftrightarrows 2H_2O \quad (1)$$

Green plants use the light-driven chemistry in PSII to carry out this process. In full sunlight, PSII oxidizes about 100 water molecules per second, which requires that 200 electron/proton pairs must be removed from substrate water each second. The electrons are used to regenerate the primary photochemistry that ultimately fixes CO_2 as biomass. The protons are released into the thylakoid lumen to form a proton gradient across the membrane that is subsequently used to drive ATP production. Five cofactors, operating in the protein milieu of PSII, are required to carry out this remarkable chemistry and handle the significant electron and proton currents associated with water oxidation. These species include (i) P_{680}, the chlorophyll complex that drives PSII photochemistry; (ii) Y_Z, a redox-active tyrosine; (iii) a cluster of four manganese ions; (iv) a Ca^{2+} ion; and (v) at least one Cl^- ion. In this review, we consider the means by which PSII catalyzes the high electron/proton flux associated with water oxidation and the functional implications that these currents have for the oxygen-evolving process. Issues pertinent to the photochemistry in PSII and to the

* Corresponding author. Fax: +1-517-353-1793; E-mail: babcock@cem.msu.edu

0005-2728/00/$ – see front matter
PII: S0005-2728(00)00069-4

internal chemistry of the $(Mn)_4$ cluster are not considered in detail.

1.1. PSII reaction-center structure

Although a high-resolution structure of PSII is not yet available, progress on both two- and three-dimensional crystals is being made ([1]; H.T. Witt, XIth International Congress in Photosynthesis, Hungary, 1998). The scheme in Fig. 1A summarizes some of the information currently available on the core PSII polypeptides and the arrangement of the cofactors described above within this protein scaffold (for reviews see [2–10]). Embedded in an array of chlorophyll/protein complexes that serve to increase light absorption, the heart of PSII comprises the D1 and D2 proteins, which bind P_{680}, the pheophytins, and the quinones that are involved in the primary photochemistry. Y_Z is located at the D1–161 position. Ligands to the $(Mn)_4$ cluster are also contained in the D1 protein, although the full ligand set for these metals has yet to be identified. Ca^{2+} and Cl^- are likely to be associated with the $(Mn)_4$ cluster. The relatively weak electronic coupling between the chlorophylls that make up P_{680} suggests that they are arranged in a less compact structure than the bacteriochlorophylls that form the special pairs in bacterial reaction centers.

Fig. 1B provides a closer view of some of the structural information available on the arrangement of the cofactors essential to water oxidation. Magnetic-resonance work and analogies to the bacterial reaction center indicate a Y_Z–P_{680} distance of about 10 Å [11,12]. Mutagenesis and kinetic data have shown that D1-H190 is hydrogen bonded to the phenol proton of Y_Z [13–17] and suggest that the imidazole group of the histidine may also hydrogen bond to D1-E189 [15]. Based on initial work from the groups of Rutherford [18] and Nugent [19], Britt and coworkers showed that Y_Z and the $(Mn)_4$ cluster are sufficiently close to constitute a single catalytic center [20,21]. The magnetic center-to-center distance between these two cofactors is 8–10 Å [22–26], but the edge-to-edge distance between Y_Z and $(Mn)_4$ may be significantly shorter. Yachandra, Sauer, and Klein have interpreted their X-ray absorption spectroscopic data to indicate that the $(Mn)_4$ cluster occurs as a dimer of μ-oxo bridged dimers arranged in an open, C-shaped geometry [5,27], although the exact structure of the cluster remains a matter of controversy. Taken together, these data suggest the close association of $(Mn)_4$, Ca^{2+}, Cl^-, Y_Z, and D1-H190 in the overall structure shown in Fig. 1B as a reasonable working model for the oxygen-evolving complex (OEC) [7,28].

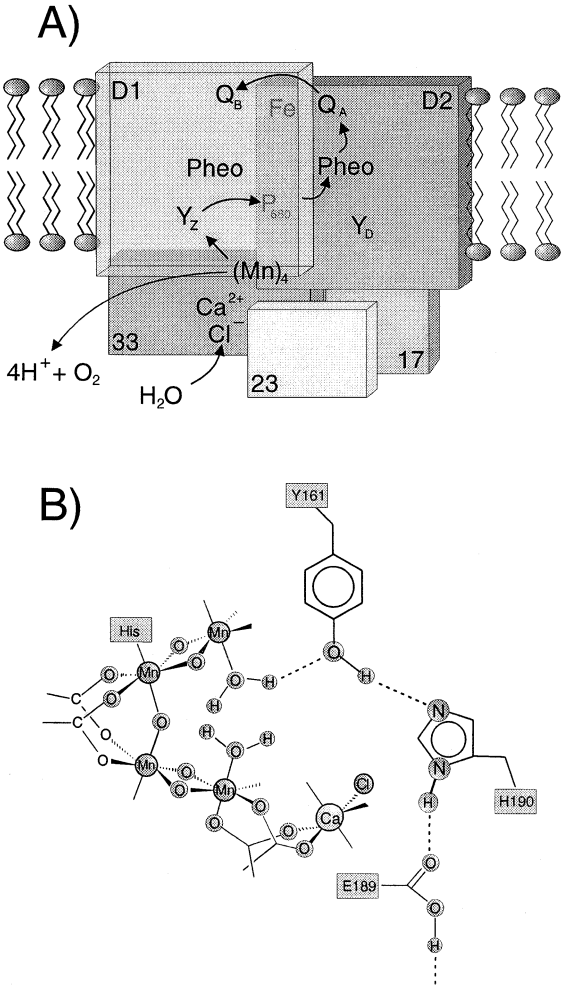

Fig. 1. (A) Schematic of the overall organization of PSII. The D1 and D2 polypeptides house the essential cofactors: P_{680}, Y_Z, the manganese cluster, Ca^{2+}, and Cl^-. (B) A postulated structure for the S_0 state in PSII that incorporates X-ray absorption data for the arrangement of the $(Mn)_4$ cluster [5,27], a close approach of Y_Z to this cluster [20–26], and hydrogen-bonding interactions between substrate water and Y_Z [7,28] and between D1-H190 and Y_Z [13–17].

1.2. Photon, electron, and proton transfers

The dynamics of photon absorption, charge sepa-

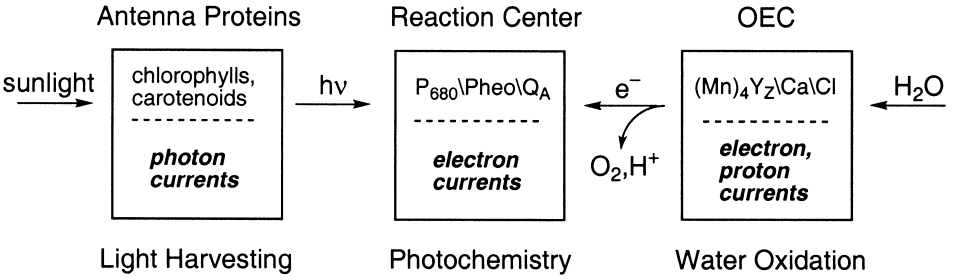

Fig. 2. An overview of the dynamic flow of photon currents, electron currents, and coupled electron/proton currents in photosynthetic water oxidation.

ration, and water oxidation in PSII are summarized in Fig. 2. The antenna proteins absorb sunlight and photon currents within these ensembles deliver light quanta on the fs and ps time scales to the reaction-center complex. Within PSII, these photons drive the primary photochemistry to generate the P_{680}^{+}/Q_A^{-} state and convert photon energy into stored chemical potential. The charge-separating photochemistry occurs on the ps time domain and involves only pure electron-transfer processes. P_{680}^{+} is reduced by Y_Z on the ns time scale as the electron/proton currents associated with water oxidation come into play. Thus, there is a graded evolution in time as photon currents are converted into electron currents and on into coupled electron/proton currents during the conversion of light energy into the stable products of photosynthesis.

1.3. The energetics of charge separation and water oxidation

PSII is driven by the 1.82 eV photons that are required to transfer P_{680} into its lowest excited singlet state. Early theoretical work by Duysens and by Ross and Calvin showed that a maximum of about two-thirds of the photon energy in photosynthesis could be converted into chemical potential in a thermodynamically efficient, charge-separation process [29,30]. These considerations indicate that the maximum potential span between P_{680}^{+} and Q_A^{-} should not exceed 1.23 V. As the potential of the Q_A/Q_A^{-} couple is on the order of -0.10 to 0 V [4], this, in turn, suggests that the potential of the P_{680}^{+}/P_{680} couple should be on the order of 1.13–1.23 V. These theoretical predictions are well in line with the $\sim$1.12 V estimate that Klimov et al. have made of the P_{680}^{+} potential and show that the PSII photochemistry operates at close to the theoretical limit (Table 1; [31]). This is clearly a triumph of evolution, but it raises the issue of how P_{680}^{+} can be so oxidizing, as the reduction potential of chlorophyll *a* in organic solvent is estimated to be ≤ 0.90 V ([32] and references therein). Williams, Allen, and their coworkers have shown recently, however, that the reduction potential of the bacteriochlorophyll special pair in *Rhodobacter sphaeroides* can be increased by at least 0.30 V when additional hydrogen-bonding interactions are designed into the bacterial reaction center [33]. These data imply that local protein effects can tune the potential of the P_{680}^{+}/P_{680} couple into the 1.10–1.20 V range that occurs in PSII.

The free energy required to carry out the four-electron oxidation of water was shown by Joliot, Kok, and their coworkers to accumulate linearly with photons absorbed [34,35]. Thus, each PSII unit operates independently in generating the four oxidizing equivalents necessary to achieve the four-electron oxidation of water shown in Reaction 1. Kok introduced the S_n notation to describe the redox state of the OEC. The subscript *n* has values between 0 and 4 and denotes the number of stored oxidizing equivalents in the OEC. Only the S_4 state has acquired the necessary four oxidizing equivalents to split water. Following the water-oxidation chemistry, the OEC is reset to the S_0 state and the linear accumulation of oxidizing equivalents with photon absorption commences anew.

The reduction potentials for the P_{680}^{+}/P_{680} couple and for the four-electron oxidation of water impose substantial restrictions on PSII. The pH in the thylakoid lumen can be as low as 5 [36], which sets the potential that must be generated to oxidize water at 0.93 V [37]. A total of 4×0.93 V = 3.72 V must be accumulated by the OEC in order to oxidize water

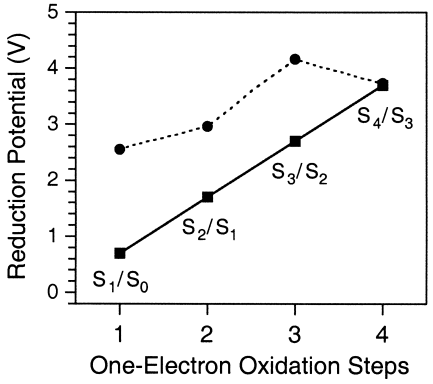

Fig. 3. Accumulated reduction potentials involved in the oxidation of two water molecules to form dioxygen. The figure shows (●) the uncatalyzed, solution potentials and (■) the potentials involved in the photosystem II catalyzed process.

reversibly. P_{680}^+ reduction proceeds with a driving force of ~1.12 V to oxidize Y_Z, which has a potential estimated at ~0.97 V (see below; Table 1). Thus, PSII supplies about 4 V to drive water oxidation. These considerations show that the water-oxidizing process occurs with little surplus energy. Tight restrictions must be in place to prevent significant variations in the potential of P_{680}, and the $(Mn)_4Y_Z$ site must be designed so that the redox properties of the metal cluster and of the tyrosine do not fluctuate substantially as the OEC proceeds through the S-state cycle. Fig. 3 illustrates the situation schematically by tracking the storage of chemical potential as photons are absorbed by PSII. The reduction potential of the S_1/S_0 pair is ~0.70 V and approximately 1 V is accumulated with each cycle of photon absorption and S-state advance (Table 1 and Fig. 3, squares and solid line). This raises an interesting problem, however, when the one-electron potentials for the oxidation of water to oxygen are considered (Fig. 3; circles and dashed line). These fluctuate dramatically as the uncatalyzed process proceeds from water to hydroxyl radical to peroxy to superoxy and, finally, to O_2. Thus, considering the fairly constant 1 V available from P_{680} and Y_Z, the $(Mn)_4$ cluster must operate in a fashion that levels these one-electron potentials for the O_2/H_2O couple. We return to these issues below.

2. Y_Z oxidation: reduction potential, kinetics, and proton currents

Y_Z has at least three functions in PSII. First, its high reduction potential preserves the strongly oxidizing conditions that are generated by the photooxidation of P_{680} and required for water oxidation. Second, Y_Z provides a quantum yield close to unity in PSII by re-reducing P_{680}^+ rapidly relative to the P_{680}^+/Q_A^- charge-recombination reaction that otherwise would dissipate the chemical potential generated by the charge separation as heat. Third, as illustrated in Fig. 2, it is at the level of Y_Z that proton currents are switched on in the evolution from energy migra-

Table 1
Redox properties of cofactors in photosystem II

Redox couple	Reduction potential	Conditions and references
P_{680}^+/P_{680}	E_m = 1.13–1.23 V	theoretical limit, see text
P_{680}^+/P_{680}	E_m = 1.12 ± 0.05 V	experimental estimate, [31]
$Y_Z^\bullet/Y_Z$	E_m = 0.97 ± 0.02	see text, [38]
S_1/S_0	$E_m \leq$ 0.70 V	[38]
S_2/S_1, S_3/S_2	E_m = 0.90–0.95 V	[38]
$Y^\bullet/Y^-$	$E_{1/2}$ = 0.68 V	aqueous, Fig. 4
$Y^\bullet/Y$	$E_{1/2}$ = 0.97 V	aqueous, pH 5.0, Fig. 4
$Y^{\bullet+}/Y$	$E_{1/2}$ = 1.38 V	aqueous, Fig. 4
O_2/H_2O	E_m = 0.93 V	aqueous, pH 5.0 [37]
Redox event	**Potential difference**	**Conditions and references**
$Y_Z \rightarrow P_{680}^+$	ΔE_m = 80–87 mV	S_0, S_1, pH 7.5, thylakoids [39]; pH 6.5, PSII cores [40]
$Y_Z \rightarrow P_{680}^+$	ΔE_m = 20–30 mV	S_2, S_3, pH 7.5, thylakoids [39]; pH 6.5, PSII cores [40]
$Y_Z \rightarrow P_{680}^+$	ΔE_m = 75 mV	apo-PSII, pH 5.0, BBYs [45]
$Y_Z \rightarrow P_{680}^+$	ΔE_m = 110–120 mV	apo-PSII, pH 6.0, BBYs [45]; PSII cores [44]

tion to electron transfer to water oxidation in PSII. In the sections that follow, we consider each of these three functions.

2.1. Preservation of high reduction potential in PSII

The reduction potential of Y_Z must remain high and essentially unaltered in the different S states (see above). A variety of data has been obtained that confirms that this is the case (Table 1). Vass and Styring estimated the potential of Y_Z as 0.95–0.99 V from steady-state redox equilibria between several PSII cofactors [38]. The kinetic potential of Y_Z has also been estimated. Thus, Brettel et al. concluded that in S_0 and S_1 the equilibrium constant, K_{ZP}, for the $Y_Z \rightarrow P_{680}^+$ reaction is 29 about 1 μs after the flash [39]. This equals a ΔE_m of 87 mV between the two redox cofactors. With a P_{680}^+/P_{680} potential of 1.12 V, a kinetic potential of 1.03 V is calculated for Y_Z in the ns time domain of the oxidation process. A similar ΔE_m for the $Y_Z \rightarrow P_{680}^+$ reaction in S_0 and S_1 has been reported recently [40]. Taken together, the 1 μs kinetic and steady-state potentials indicate a further relaxation of 40–80 mV in the Y_Z midpoint on the μs time scale. Although the potentials for Y_Z given above were obtained at different pH values in different preparations, the measurements were performed under conditions optimized for high rates of O_2 evolution. Consequently, the estimated Y_Z potentials are at a pH close to the operational value. For S_2 and S_3, K_{ZP} was estimated as 2–4 at 1 μs after the flash, which decreases the ΔE_m between P_{680} and Y_Z to 20–30 mV [39,40]. Above 1 μs there is further evolution in the Y_Z/P_{680}^+ equilibrium. This effect is more pronounced in the higher S states and most likely accounts for the greater μs amplitude in P_{680}^+ reduction in S_2 and S_3 (see below). The decrease in K_{ZP} in the higher S states can represent a shift in potential in either P_{680} or Y_Z or both. Nonetheless, and as noted by Ahlbrink et al. [40], the observed shift in the ΔE_m between the lower and higher S states is only about 50 mV. These results demonstrate the redox stability of P_{680} and Y_Z as the S states clock through their cycle. Such stability would not be expected, however, if an uncompensated positive charge is being accumulated at the $(Mn)_4$ cluster during the $S_1 \rightarrow S_2$ transition, as suggested from measurements on proton release and spectral bandshifts (see below; [41–43]). This is particularly so, considering the compact geometry predicted for the cofactors on the donor side of PSII (Fig. 1B), and thus, we have argued elsewhere [7] that dipole change, but not charge accumulation, occurs during $S_1 \rightarrow S_2$. The ΔE_m between P_{680} and Y_Z has been estimated in the μs time scale in apo-PSII samples, which lack the $(Mn)_4$ cluster and the extrinsic proteins. These values are 75 and 115 mV at a solution pH of 5 and 6, respectively [44,45].

Thus, the ΔE_m for the $Y_Z \rightarrow P_{680}^+$ reaction remains relatively constant, independent of S state and the presence or absence of the $(Mn)_4$ cluster. There has been considerable recent debate, however, as to the protonation state and hydrogen-bonding status of the oxidized and reduced forms of Y_Z and of the fate of any protons that are released during the oxidation of the side chain. To begin the discussion of these issues, which are essential to resolve in order to understand the energetics of Y_Z oxidation described above, we summarize the redox reactions of tyrosine dissolved in water and when the aromatic residue is transferred to a protein milieu in Table 2. We first discuss the energetics of these processes and then apply the insights that result in interpreting recent observations on PSII.

2.1.1. Redox properties of tyrosine in solution and in PSII

Fig. 4 shows the aqueous solution potential of tyrosine as a function of pH. This behavior is described by the relation:

$$E_{1/2} = E_{1/2}(Y^{\bullet+}/Y) + 0.059 \log\left[\frac{10^{-pH} + 10^{-pK_{red}}}{10^{-pH} + 10^{-pK_{ox}}}\right] \quad (2)$$

where pK_{red} and pK_{ox} represent the acid dissociation constants of the reduced and oxidized form of the aromatic side chain, respectively [46]. Tyrosine can undergo three different redox events in water, depending on the pH (Table 2). Above $pH = pK_{red} = 9.9$, the $Y^{\bullet}/Y^-$ redox couple has a pH-independent potential of 0.68 V. In the region, $pK_{ox} < pH < pK_{red}$, the neutral $Y^{\bullet}/Y$ pair is the relevant redox couple and has a pH-dependent potential that increases by 59 mV per pH unit. The $Y^{\bullet}/Y$ couple has a potential of 0.97 V at pH 5.0. Finally, the

pH-independent, 1.38 V potential of the $Y^{\bullet+}/Y$ redox couple was estimated by fitting the data in Fig. 4 with Eq. 2 and assuming a pK_{ox} of −2 for tyrosine [47]. The 1.12 V P_{680}^{+}/P_{680} potential, and the 0.93 V potential that represents the average, one-electron solution potential of the O_2/H_2O redox pair at pH 5.0, are also shown in Fig. 4. The potentials of the different redox couples in Fig. 4 are summarized in Table 1.

The redox properties of a tyrosine buried within a protein are more complex and four different couples must be considered (Table 2). The potential of the $Y^{\bullet+}/Y$ redox couple, which is 1.38 V in water (Fig. 4), will increase further in the low dielectric medium of a protein, unless there are compensating negative charges in the vicinity. We can roughly estimate the effect of the protein dielectric on this potential by using the Born model:

$$\Delta G = \frac{14.397}{\varepsilon r} \quad (3)$$

where ΔG (V) represents the electrostatic penalty incurred by introducing a charged species with radius r (Å) in a medium with a homogeneous dielectric constant ε ([48] and references therein). Assuming an average radius of 3 Å for the aromatic ring, the $Y^{\bullet+}/Y$ potential is predicted to increase to 1.80–1.92 V when the tyrosine is transferred from water, with a dielectric of 80, into a protein with an ε of 8–10, as recently suggested for PSII [32]. The potential will increase further, if the dielectric is lower at the $(Mn)_4Y_Z$ site. Blomberg et al. reached similar conclusions from a quantum mechanical analysis of tyrosine oxidation [49]. These theoretical predictions are consistent with recent work that showed that the potential of a tyrosine buried within the hydrophobic core of a de novo protein is increased dramatically relative to the solution potentials in Fig. 4 [50].

Table 2
Redox properties of tyrosine in aqueous and proteinous media

Tyrosine redox couples in water	Conditions
$Y^- \rightarrow Y^{\bullet} + e^-$	$pH > pK_{red}$
$Y \rightarrow Y^{\bullet} + H^+ + e^-$	$pK_{ox} < pH < pK_{red}$
$Y \rightarrow Y^{\bullet+} + e^-$	$pH < pK_{ox}$
Tyrosine redox couples in a protein	
$Y^- \rightarrow Y^{\bullet} + e^-$	$pH > pK_{red}$
$Y \rightarrow Y^{\bullet} + H^+(\text{protein}) + e^-$	$pK_{ox} < pH < pK_{red}$
$Y \rightarrow Y^{\bullet} + H^+(\text{bulk}) + e^-$	$pK_{ox} < pH < pK_{red}$
$Y \rightarrow Y^{\bullet+} + e^-$	$pH < pK_{ox}$

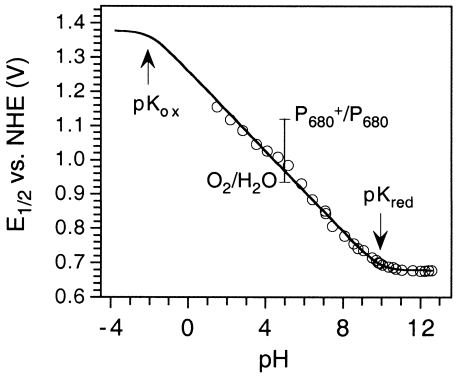

Fig. 4. $E_{1/2}$ potentials derived by differential pulse voltammetry (DPV) on tyrosine as a function of pH. The fit to the data is described by Eq. 2. Experimental conditions: sample, 0.35 mM *N*-acetyl-L-tyrosinamide in a 10 mM potassium phosphate, 200 mM KCl solution; scan rate, 10 mV s^{-1}; sample width, 17 ms; pulse amplitude, 50 mV; pulse width, 50 mV; pulse period, 200 ms; temperature, 22°C. The $E_{1/2}$ values were obtained from irreversible DPV traces [50] and calculated by $E_{1/2} = E_P + (\text{pulse amplitude}/2)$. The ferricyanide/ferrocyanide redox pair was used as an internal standard. The potentials of the P_{680}^{+}/P_{680} and O_2/H_2O redox couples are also shown.

In a protein, redox Bohr effects could lower the $Y^{\bullet+}/Y$ potential by electrostatic relaxation of peripheral amino acids. For example, Rappaport and Lavergne demonstrated an amino-acid pK_a shift from 8.20 to 7.25 in the $S_1 \rightarrow S_2$ transition [51], which represents an electrostatic relaxation of 56 mV. In the bacterial reaction center, the formation of Q_A^- and Q_B^- produce pK_a shifts of 1.5–2.0 units [52], which equal 0.09–0.12 V. These values are typical for electrostatic relaxation in membrane proteins and indicate that redox Bohr effects on the donor side of PSII will, at most, lower the $Y^{\bullet+}/Y$ potential to 1.68–1.83 V. This value is still 0.56–0.71 V higher than the P_{680}^{+}/P_{680} redox couple. Taken together, these considerations provide strong arguments that exclude the formation of a tyrosine cation radical in PSII as a thermodynamically viable intermediate. A cation radical is not likely to occur even as a thermally activated, transient state in the electron transfer between P_{680} and the $(Mn)_4$ cluster. This is evident from the observation that $Y_Z^{\bullet}$ can be detected as a transient intermediate at high concentration during catalysis and, moreover, from the fact that Y_Z is oxidized by P_{680}^{+} even when the electron-transport

chain is terminated after the tyrosine by depletion of the $(Mn)_4$ cluster.

Consistent with this analysis, a variety of data has shown that Y_Z is a deprotonated, neutral radical in its oxidized state. The *g*-value of the EPR spectrum [53] and the radical spin-density distribution [54] are characteristic of a neutral radical. Moreover, a recent FTIR study of $Y_Z^{\bullet}$ showed that this species has vibrational properties typical of a neutral radical [55]. Optical data have also been interpreted along these lines [56–58]. Finally, site-directed mutagenesis [13–17] and chemical rescue [16] studies have shown that the D1-H190 provides a base function that is essential for effective oxidation of Y_Z. These results are all consistent with a model in which the phenol proton either leaves simultaneously with the electron upon oxidation of the tyrosine or that Y_Z is involved in a proton pre-equilibrium with its hydrogen-bonding partner, D1-H190 (see below).

2.1.2. Protonation state and pK_{red} of reduced Y_Z

Fig. 4 demonstrates that the potential of the $Y^{\bullet}/Y^{-}$ redox pair is 0.68 V in water, which is too low for the water-splitting reactions in PSII. This redox couple can only be operational in water oxidation if pK_{red} for the tyrosine is downshifted to ~ 5, which requires a significant effect of the protein on the acid/base properties of the side chain. The protonation state of reduced Y_Z has been probed by using difference FTIR [55] and optical [56–58] spectroscopies. The optical work relies on comparisons of difference spectra for Y_Z in its oxidized and reduced states to those of phenolic compounds in solution and in other proteins. The FTIR approach is more direct, as it monitors the occurrence of the phenol C-O-H bending mode, which can only be observed if the tyrosine is protonated. Candeias et al. and Haumann et al. conclude that Y_Z is a tyrosinate in the active form of the enzyme from their optical comparisons [56,58]. There are difficulties with this interpretation, however, as the pH dependence of the optical difference spectra reported by Haumann et al. [58] is opposite to that reported by Diner and coworkers [57]. Moreover, the optical difference spectra reported by Candeias et al. and interpreted as indicating that Y_Z occurs as a tyrosinate in Mn-depleted preparations [56] are in conflict with FTIR data on directly comparable samples that clearly show the C-O-H bending mode [55]. Ambiguities with the optical data most likely arise from the fact that this technique is indirect and influenced by a number of factors, in addition to the protonation state of the tyrosine phenol oxygen. The observation of the hydroxyl bending mode by FTIR, on the other hand, provides straightforward support for the occurrence of the protonated tyrosine, rather than the deprotonated tyrosinate, as the active Y_Z species in P_{680}^{+} reduction.

The protonation state and pK_{red} value of Y_Z have also been investigated by kinetic measurements. Rappaport and Lavergne studied the rate of $Y_Z^{\bullet}/Q_A^{-}$ recombination in apo-PSII and concluded that this reaction is modulated by a base with an apparent $pK_a \sim 6.0$ [59]. Ahlbrink et al. used optical spectroscopy to examine the characteristics of the $Y_Z \rightarrow P_{680}^{+}$ reaction as a function of pH in both apo- and intact PSII [40]. These authors proposed that Y_Z oxidation is rate-limited by proton transfer below pH 7.0 and by electron transfer above this pH in apo-PSII. The apparent pK_a of ~ 7.0 was proposed to reflect either the pK_a of the proton-accepting base that is hydrogen bonded to Y_Z or the pK_{red} of Y_Z itself. A similar situation was envisioned in the intact enzyme but with an operational pK_a of 4.5. In a more recent study from the Junge group, the oxidized-minus-reduced optical difference spectrum was used to suggest that Y_Z is a hydrogen-bonded tyrosinate in the active enzyme [58]. The interpretation of such spectra is problematic, however, as described above. Diner et al. investigated the pK_{red} of Y_Z in apo-PSII samples by studying the optical difference spectrum and by measuring the pH dependence of the rate of Y_Z oxidation and of the deuterium isotope effect on this reaction [57]. Based on these studies, and on the observation that the C-O-H bending mode in the $Y_Z^{\bullet}$-Y_Z FTIR spectrum disappears between pH 8 and 9 (unpublished, but cited in Ref. [57]), Diner and coworkers proposed a pK_{red} of 8.0–8.3 for Y_Z in apo-PSII. A similar pK_{red} value of 8.1 for Y_Z was estimated by Mamedov et al. by studying chlorophyll fluorescence kinetics in dark-grown, Mn-deficient D1-H190 mutants [17].

Whether these relatively low pK_{red} values occur for Y_Z in apo-PSII has recently been examined by Debus and coworkers. In their initial work, Hays et al. [16] showed that Y_Z cannot reduce P_{680}^{+} effectively at neu-

tral pH when D1-H190 is mutated to an amino acid unable to accept the proton released upon Y_Z oxidation (see also [13–15]). They showed further that imidazole and other small organic bases are able to chemically rescue D1-H190 mutants and restore rapid P_{680}^+ reduction by entering the Y_Z site and accepting the phenol proton that is mobilized as Y_Z is oxidized. In their most recent study [60], they measured the rate of P_{680}^+ reduction in a D1-H190A mutant and observed an apparent pK_a of 10.3. In the presence of ethanolamine or imidazole, this value shifted to 9.5 and 6.9, respectively, which are the solution pK_a's of these two bases. Thus, in the presence of an exogenous base in the D1-H190A mutants, the apparent pK_a for the rate of the $Y_Z \rightarrow P_{680}^+$ electron transfer tracks with the pK_a of the base that accepts the proton upon Y_Z oxidation. This observation is consistent with scheme 1A in Ahlbrink et al. [40] in which the observed pK_a of $\sim$7.0 in the wild-type system corresponds to the pK_a of D1-H190. In the D1-H190A mutant in the absence of exogenous bases, Hays et al. assigned their apparent pK_a of 10.3 to Y_Z itself [60], which is close to the 9.9 value for tyrosine in water (Fig. 4). A pK_{red} of 10.3 does not necessary contradict the FTIR data [55,57], as the IR feature assigned to the C-O-H bending mode is weak and could be broadened beyond detection at high pH.

We conclude that the pK_{red} value of Y_Z is between 8.0 and 10.3 in apo-PSII, with a refinement of this value expected in the near future. FTIR data on inhibited PSII preparations that retain the $(Mn)_4$ cluster indicate that the vibrational properties of Y_Z, including the C-O-H bending mode, are similar to those in metal-depleted centers [55,57]. The acid-base properties of Y_Z in the fully functional enzyme, however, have not been assessed. The work described above shows that, in measurements of the $Y_Z \rightarrow P_{680}^+$ reaction rate, the pK_{red} of Y_Z is masked by the pK_a of the base that accepts the phenol proton during Y_Z oxidation. Optical spectroscopy is the only technique applied thus far that has sufficiently high time resolution and signal-to-noise ratio to obtain a difference spectrum for Y_Z in the active enzyme. Although this measurement has the potential to assess pK_{red} for Y_Z, the interpretation of these spectra in terms of the protonation state of Y_Z is ambiguous. Time-resolved FTIR will most likely be necessary to determine this pK_{red} value and thus provide insight into the protonation state of Y_Z in the active enzyme. Nonetheless, some predictions can be made for the oxygen-evolving system. The energetics in Fig. 4 show that, unless there are positive charges in the vicinity Y_Z that lower its pK_{red} to $\sim$5 or less, $Y_Z^\bullet/Y_Z^-$ is not the functional redox couple in PSII. We consider it unlikely, however, that protein side chains will be ionized in the Y_Z site. The occurrence of charge will modulate the reduction potential of the tyrosine, as well as its pK_{red}, and make it difficult to maintain the stable reduction potential that is critical for efficient O_2 evolution. Therefore, Y_Z is likely to occur as a protonated tyrosine in active centers and to be oxidized to a neutral radical by P_{680}^+.

2.1.3. *The influence of proton currents on the reduction potential of Y_Z*

The potential required to oxidize tyrosine to its neutral radical in a protein depends on the fate of the proton released during the oxidation process (Table 2). One scenario is that the phenol proton is solvated within the low dielectric medium of the protein. A second possibility is that the proton is released into bulk solution. Fig. 5 provides a description of these possibilities in PSII as follows: (A) the phenol proton is transferred to H190 upon oxidation of Y_Z, (B) the proton is distributed over several acceptors, or (C) oxidation of Y_Z gives rise to domino deprotonation through a network of proton acceptors that ultimately releases a proton to bulk. Below, we discuss the energetics for these three models.

Fig. 5A shows a model in which the phenol proton, and the charge associated with it, remains on H190 following Y_Z oxidation. By using Eq. 3, and assuming an average radius of 4.0 Å for a hydrogen-bonded tyrosine/histidine complex, the potential of the $Y^\bullet/Y$ redox couple is estimated as 1.28–1.37 V at pH 5.0 in a protein with an ε of 8–10. If the dielectric constant is 4 at the $(Mn)_4Y_Z$ site, the potential increases to 1.82 V. Even if a redox Bohr relaxation of 0.12 V is included in the calculation, the estimated tyrosine potential remains $\geq$1.16 V. Thus, it is unlikely the H190 forms a stable imidazolium cation during the lifetime of $Y_Z^\bullet$. The results from the D1-H190 mutants provide strong evidence that this residue serves as the proton acceptor upon Y_Z oxidation [13–17,60]. This is further supported by

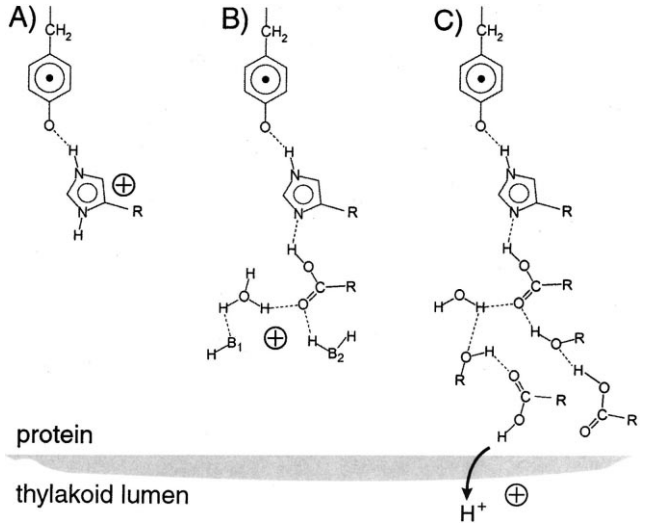

Fig. 5. Possible events in PSII upon oxidation of Y_Z. (A) The phenol proton is transferred to D1-H190. (B) The phenol proton is distributed over several acceptors. (C) Oxidation of Y_Z gives rise to domino deprotonation through a network of proton acceptors that ultimately releases a proton to the lumen.

analogy to D2, where a hydrogen bond between D2-H189 and Y_D, in both its reduced and oxidized form, has been shown [61–64]. Together these results predict that H190 accepts the phenol proton upon oxidation of Y_Z but, in turn, deprotonates from the second nitrogen of the imidazole ring and remains neutral. This proposal is consistent with the model presented by Rappaport and Lavergne in which the Y_Z proton remains close to $Y_Z^{\bullet}$ but shifts the pK_a of a nearby base from ≥ 9 to 6 [59]. This conclusion, however, is counter to proposals that are based on transient spectral bandshifts that occur during the Y_Z redox cycle. These absorption changes have been interpreted to reflect the creation of uncompensated charge in the immediate vicinity of the tyrosine radical upon its oxidation by P_{680}^+ [41,43,59,65]. Alternative explanations of the chlorophyll bandshifts are possible, however, that remove the necessity of forming and quenching charge upon each redox cycle of Y_Z, as discussed in [66] and below.

If the phenol proton is distributed over several bases, as shown in Fig. 5B, the potential of the tyrosine will be lower than in the localized situation in Fig. 5A. Eq. 3 predicts that the volume of the proton-acceptor cluster will modulate the tyrosine potential and allows an estimate of the size of the base cluster required to satisfy the constraints on Y_Z oxidation in PSII. These considerations are consistent with ab initio calculations on the ionization potential of Y_Z, which was shown to decrease as the size of the proton-acceptor chain increased [49]. Assuming a 0.97 V potential for Y_Z and redox Bohr effects of ≤ 0.12 V, Eq. 3 predicts that the phenol proton can be buried within PSII if the electrostatic penalty is 0.12 V or less. This condition requires that the phenol proton be distributed over a cluster of proton acceptors with an average diameter on the order of 20 Å in a dielectric of 8–10. If the dielectric is 4, the proton-acceptor cluster must be >50 Å in diameter, before Y_Z oxidation becomes thermodynamically feasible.

The third possibility for PSII is that the proton migrates out to the thylakoid lumen, as illustrated in Fig. 5C. In this case, the potential of the tyrosine in the protein should be the same or very close to the aqueous solution value, assuming that the hydrogen-bonding properties of the aromatic side chain are similar in the two different media. This is likely to be the situation for Y_Z since it has been shown to be hydrogen bonded in both its reduced and oxidized form (e.g. [55]), as predicted for tyrosine in water. Thus, this model predicts that Y_Z has a potential of $\sim$0.97 V at pH 5.0, which is consistent with the experimentally determined value (Table 1). This model also predicts that there may be a time evolution in the potential of Y_Z. As the proton migrates through the protein to bulk, the potential of Y_Z is expected to relax toward the $\sim$0.97 V value. Experimental data that suggest such a time evolution in potential are discussed below. Finally, Fig. 5C does not require that the specific phenol proton on Y_Z migrates all the way to bulk during the oxidation process. Rather, we suggest that proton release to solution reflects domino deprotonation in which the tyrosine is oxidized and protonates H190, which, in turn, releases a proton to, for example, E189 and so on.

2.2. Preservation of quantum yield in water oxidation

The second key function for Y_Z is that it preserves a quantum yield close to unity for charge separation in PSII. Y_Z is oxidized on the ns time scale, which is fast relative to the 200–400 μs electron transfer from Q_A^- to Q_B [2–4]. More importantly, Y_Z oxidation is

also fast with respect to the recombination of Q_A^- with P_{680}^+, which takes place with time constants of 200–1000 μs, depending on the sample preparation and organism [2–4,44]. These kinetic comparisons emphasize that the high rate of P_{680}^+ reduction by Y_Z, relative to these other processes, is the event that locks in the high quantum efficiency of the primary charge separation in PSII.

2.2.1. Oxidation of Y_Z on the ns time scale in active PSII

The $Y_Z \rightarrow P_{680}^+$ reaction exhibits S-state-dependent, multiphasic electron-transfer kinetics in active PSII, as shown in Table 3. Although the kinetic information has been derived primarily by monitoring P_{680}^+ reduction, Y_Z is the only redox cofactor between P_{680} and the $(Mn)_4$ cluster [44,67–70]. The major population of P_{680}^+ is reduced in the ns time domain. The main kinetic phase is 20–40 ns in S_0 and S_1 at pH 7–4 [39,71]. P_{680}^+ reduction becomes biphasic in the presence of S_2 and S_3 with components of about 50 ns and 280 ns at pH 7–4 [39,71]. Eckert and Renger studied the temperature dependence of P_{680}^+ reduction in the ns time domain and derived an activation energy of ~0.10 eV in the S_1 state at pH 6.5 over the temperature range −25 to 22°C [72]. A smaller, ~20%, fraction of P_{680}^+ is reduced on the μs time scale. The halftimes of these slower kinetic components are in the range of 1–35 μs and their amplitudes oscillate as a function of the redox state of the $(Mn)_4$ cluster, which strongly suggests that they are associated with $Y_Z \rightarrow P_{680}^+$ in samples fully active in water oxidation [73–78]. H/D isotope effects on P_{680}^+ reduction have been studied in both the ns and μs time domains. The ns reduction kinetics remain essentially the same in D_2O [75,79,80]. In contrast, a significant isotope effect accompanies the μs phases [75,77].

The kinetic expression advanced by Dutton, Moser, and coworkers for estimating the rates of intraprotein electron-transfer reactions can be used to gain insight into the nature of Y_Z oxidation. The relationship developed by the Dutton group is described by:

$$\log k_{et} = 13 - [(1.2 - 0.8\rho)(R - 3.6)] - 3.1\frac{(\Delta G + \lambda)^2}{\lambda} \quad (4)$$

where k_{et} represents the exergonic electron tunneling rate (s^{-1}), ρ is the specific packing density of the

Table 3
Properties of electron-transfer reactions in photosystem II

Electron transfer reaction	Electron transfer rate	Conditions and references
$Y_Z \rightarrow P_{680}^+$	$t_{1/2}$ = 20–40 ns	S_0, S_1, pH 7–4, PSII cores [39,71]
$Y_Z \rightarrow P_{680}^+$	$t_{1/2}$ = 50/280 ns	S_2, S_3, pH 7–4, PSII cores [39,71]
$Y_Z \rightarrow P_{680}^+$	$t_{1/2}$ = 1–35 μs	[73–78]
$Y_Z \rightarrow P_{680}^+$	$t_{1/2}$ = 2–44 μs	apo-PSII, pH 9–4, chloroplasts [90]
$Y_Z \rightarrow P_{680}^+$	$t_{1/2}$ = 160 μs	-Ca^{2+},Cl^-, S_1, S_2, pH 5.5, PSII cores [102]
$Y_Z \rightarrow P_{680}^+$	$t_{1/2}$ = 10–40 μs	-Ca^{2+}, S_1, S_2, pH 6.5, BBYs [103]
$Y_Z \rightarrow P_{680}^+$	$t_{1/2}$ = 35 ns	-Cl^-, S_1, pH 6.5, PSII cores [105]
$Y_Z \rightarrow P_{680}^+$	$t_{1/2}$ = 35/100 ns	-Cl^-, S_2, pH 6.5, PSII cores [105]
Electron transfer reaction	**H/D isotope effect**	**Conditions and references**
$Y_Z \rightarrow P_{680}^+$	$K_H/K_D = \leq 1.1$	ns phases [75,79,80]
$Y_Z \rightarrow P_{680}^+$	$K_H/K_D = > 1.0$	μs phases [75,77]
$Y_Z \rightarrow P_{680}^+$	K_H/K_D = 2.7	apo-PSII, pH 6.5, BBYs [83]
$Y_Z \rightarrow P_{680}^+$	K_H/K_D = 2.5	apo-PSII, pH 5.0, PSII cores [40]
$Y_Z \rightarrow P_{680}^+$	K_H/K_D = 2.8–1.1	apo-PSII, pH 5.5–9.5, PSII cores [57]
$Y_Z \rightarrow P_{680}^+$	K_H/K_D = 1.7–2.6	apo-PSII, pH 5.0–10, PSII cores [60]
Electron transfer reaction	**Activation energy**	**Conditions and references**
$Y_Z \rightarrow P_{680}^+$	E_A = 0.10 eV	S_1, pH 6.5, BBYs [72]
$Y_Z \rightarrow P_{680}^+$	E_A = 0.48 eV	apo-PSII, pH 7.0, chloroplasts [91]
$Y_Z \rightarrow P_{680}^+$	E_A = 0.28 eV	apo-PSII, pH 6.5, BBYs [83]
$Y_Z \rightarrow P_{680}^+$	E_A = 0.30 eV	apo-PSII, pH 5.0, PSII cores [40]

inter-cofactor protein volume, R is the center-to-center distance between the closest edge atoms of the cofactors (Å), ΔG is the driving force (eV), and λ is the reorganization energy (eV) [81,82]. Eq. 4 can predict whether the fast, 20–40 ns phase in the $Y_Z \rightarrow P_{680}^+$ reaction corresponds to pure electron tunneling. For this analysis, we assume a ρ of 0.70–0.80 for the protein medium between Y_Z and P_{680}. This assumption is based on a comprehensive study of the crystal structures of electron-transfer proteins by Page et al. [82] that showed that $\sim$40% of these proteins have a ρ in this range. We take $R = 9.5$ Å, which represents the edge-to-edge distance between Y_Z and the closest chlorophyll macrocycle in PSII, on the basis of the model developed by Svensson et al. [12]. This number is consistent with Y_Z-P_{680}^+ distance estimates derived from EPR measurements [11]. Finally, we adopt a ΔG of -85 meV, which is the free-energy difference between P_{680} and Y_Z in the lower S states (Table 1). With the R and ΔG values given above and a ρ equal to 0.70–0.75, the calculated electron tunneling rate equals 20–40 ns for electron transfer between Y_Z and P_{680}^+, if λ in the range of 0.70–0.88 eV is used. We can compare these numbers to λ estimated from the activation energy, E_A, measured for the $Y_Z \rightarrow P_{680}^+$ reaction in the S_1 state according to:

$$E_A = \left[\frac{(\Delta G + \lambda)^2}{4\lambda}\right] - 1/2RT \quad (5)$$

With an E_A of 0.10 eV and a ΔG of -85 meV (Tables 1 and 3), $\lambda = 0.61$ eV. This value is close to the 0.70–0.88 values above. If the specific packing density is increased to 0.80, $\lambda = 0.61$ eV predicts an electron tunneling rate of 4 ns, which is an order of magnitude faster than the measured rate. Even if the edge-to-edge distance between Y_Z and P_{680}^+ is increased by 1.0 Å, the calculated rates are still found to be close to the experimental values, when using reasonable values of λ. Thus, with $R = 10.5$ Å and $\rho = 0.75$, a 20–40 ns rate predicts a λ of 0.59–0.68. We conclude that, within a theoretical framework of non-adiabatic electron transfer, the fast oxidation phase of Y_Z is likely to be rate limited by pure electron tunneling. Similar conclusions were recently reported by Renger et al. [83].

2.2.2. *The effects of proton coupling on electron-transfer rates and mechanisms*

The observation of multiphasic Y_Z reduction of P_{680}^+ in water-splitting PSII centers and the varying deuterium kinetic isotope effects for the different phases was surprising and intriguing. Several groups, including those of Debus, Diner, Junge, Rappaport, and Renger have addressed and clarified these processes [57–60,75–78]. To discuss the situation in PSII, we acknowledge the strong potential-surface dependence for proton transfer and summarize four different ways by which proton-coupled electron transfer (pcet) may occur [57,60]: (i) pcet in which the proton acceptor and donor have similar pK_as and are strongly hydrogen bonded; (ii) pcet in which the ΔpK_a is greater, but the donor/acceptor pair is still optimally hydrogen bonded; (iii) pcet in which the proton acceptor is weakly or not hydrogen bonded to the donor; and (iv) pcet in which the electron donor must first deprotonate through an energetically unfavorable equilibrium process.

The first three scenarios are summarized by the potential surfaces in Fig. 6. For a strong hydrogen bond between donor and acceptor groups with the same pK_a values (Fig. 6A), the barrier to proton

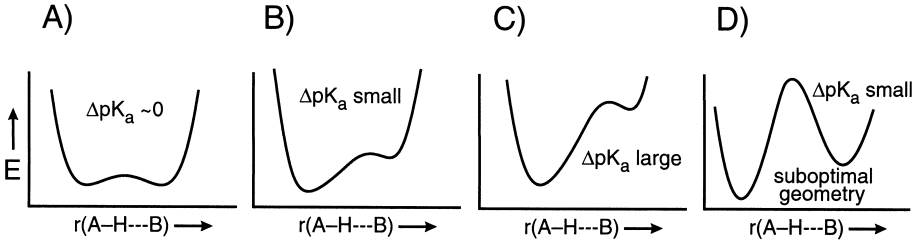

Fig. 6. Hydrogen-bond potential energy surfaces for various pK_a values of the donor and acceptor groups and for different hydrogen-bond geometries. In (A)–(C), an optimal hydrogen bond forms between donor and acceptor groups that have the same pK_a's (A), a small ΔpK_a (B), or a large ΔpK_a (C). In (D), a suboptimal hydrogen-bond geometry occurs for donor and acceptor groups with different pK_a's.

transfer is small and will not influence the rate significantly. As the pK_a's for the donor/acceptor pair diverge in the strong hydrogen-bond limit, the activation energy for proton transfer increases. Previous authors have linked the barrier directly to the pK_a difference by invoking the following equation [57,78]:

$$k_{pt} = 6\times10^{12}\times10^{\Delta pK_a} \quad (6)$$

where 6×10^{12} s^{-1} is the pre-exponential factor, $\Delta pK_a = pK_a(\text{acceptor}) - pK_a(\text{donor})$, and k_{pt} is the observed rate of the proton transfer. In Fig. 6B, the potential surface for the strong hydrogen-bond case is shown for a fairly small ΔpK_a. This situation may hold for PSII, if Y_Z is directly involved in a strong hydrogen bond with H190. Under these circumstances, ΔpK_a is on the order of -3 to -4 and proton-transfer halftimes of 0.1–1.0 ns are predicted. These are fast with respect to the $Y_Z \rightarrow P_{680}^+$ electron-transfer (Table 3) and indicate that the reduction reaction may proceed without significant proton limitation. Consistent with this, O'Malley has used computational methods to show that there is little barrier to phenol proton transfer to a histidine during its oxidation [84]. If a poorer base is incorporated into the H190 position by mutagenesis, or if water enters the site through a perturbation to the preparation and interacts with the phenol proton directly, then Fig. 6C describes the situation, provided that an optimal hydrogen bond geometry is maintained. Here, the difference in pK_a is greater, and accordingly, the rate of the proton transfer slows substantially. Taking the pK_{red} of Y_Z as 10 (Fig. 4), and the rate of the P_{680}^+/Q_A^- recombination as 200 μs, the rate of forward, pcet from Y_Z becomes comparable to that of the recombination reaction for acceptor pK_a's of 1 or less.

Eq. 6 does not take into account work on proton tunneling that shows that, even if there is a modest activation barrier, proton transfer may still be fast relative to electron transfer and obscure H/D isotope effects [85–87]. Thus, proton tunneling relaxes the requirement that hydrogen bonding must be optimized to minimize barrier height and conclusions reached regarding Fig. 6B,C hold, even if the hydrogen bond potential surface deviates somewhat from the 'strong' hydrogen bond limit. If, however, there is a significant perturbation to the potential surface by elongation or distortion of the hydrogen bond, then a significant barrier develops between the donor and acceptor potential wells [85–87]. This is the third scenario noted above and is represented by Fig. 6D. As the geometry of the hydrogen bond degrades from optimal, retardation in the proton-transfer rate becomes significant and may limit the electron transfer, despite a favorable ΔpK_a for the donor/acceptor pair. In this scenario, a detectable deuterium isotope effect is expected, owing to the difference in Broglie wavelength between the proton and the deuteron and the necessity of tunneling to pass from donor to acceptor wells.

The fourth situation has been discussed by Graige et al. [88] for the quinone complex in the bacterial reaction center and, more recently, by Diner, Debus, and their respective coworkers [57,60] for the oxidation of Y_Z in PSII. If an unfavorable protonic equilibrium is required to generate the active electron-transfer species, proton coupling is manifest in the reaction rate. We illustrate this case by considering a situation in which the tyrosinate species, $Y(O)^-$, is the actual electron-transferring component in the reduction of P_{680}^+, and that this species is generated by an equilibrium in which a base, B, accepts the phenol proton as follows:

$$Y(OH) + B \leftrightarrows Y(O)^- + B(H)^+ \quad (7)$$

The equilibrium constant for this process, K_{eq}, acts as an unfavorable multiplier on the total Y(OH) concentration and can slow the forward, proton coupled electron-transfer process appreciably from that expected for the pure $Y(O)^-$ electron donor. This scheme can be extended to provide insight into the effect of a hydrogen-bonded network on observed electron-transfer kinetics. If the proton must migrate from $B(H)^+$ to a second base, B′, to achieve favorable thermodynamic conditions for $Y(O)^-$ oxidation, then the following equilibrium holds:

$$[Y(O)^-\cdots B(H)^+] + B' \leftrightarrows [Y(O)^-\cdots B] + B'(H)^+ \quad (8)$$

In this case, a second equilibrium, $K_{eq'}$, also acts as a multiplier on the total Y(OH) concentration, and depending on its value, can slow the electron-transfer process further. Moreover, such migration through a hydrogen-bonded network can easily lead to multiphasic electron transfer kinetics, depending on the protonation state of the components of the network

prior to flash activation of PSII. The four scenarios described above are likely to be involved in PSII electron-transfer chemistry under various conditions of PSII integrity and mutagenetic state. We consider these in discussing further the proton-coupled, electron-transfer chemistry involving Y_Z.

2.2.3. Oxidation of Y_Z on the μs time scale in active PSII

The 20–40 ns phase of P_{680}^+ reduction by Y_Z in oxygen-evolving preparations is likely to reflect the situation shown in Fig. 6B, as electron tunneling appears to rate limit this process. The multiphasic nature of the $Y_Z \rightarrow P_{680}^+$ reaction indicates that this fast initial phase is followed by subsequent relaxation processes that determine the overall extent of reduction of the reaction-center chlorophyll complex by the tyrosine. The H/D isotope effects observed for the μs components suggest that proton movements are associated with the slower electron-transfer processes. Schilstra et al. [75] and Renger and coworkers [76–78] have reinvestigated the reduction of P_{680}^+ by Y_Z recently. The scheme proposed by these authors can be described as:

$$Y_Z/P_{680}^+ \xrightarrow{ns} [Y_Z^{ox}/P_{680}]_{initial} \xrightarrow{\mu s} [Y_Z^{ox}/P_{680}]_{final} \quad (9)$$

where the initial state is formed within ns and the final state is achieved as further stabilizing reactions that involve protonic equilibria occur. The PSII energetics, tyrosine redox properties, and pcet considerations above provide some insight into the chemical nature of the initial and final states in Eq. 9. The theoretical limit for the P_{680}^+/P_{680} potential, 1.13–1.23 V, is much lower than that of a tyrosine cation radical (Table 1). Thus, a $[Y_Z(OH)/P_{680}^+] \rightarrow [Y_Z(OH)^+/P_{680}]_{initial}$ equilibrium is unlikely. Even $[Y_Z(OH)/H190/P_{680}^+] \rightarrow [Y_Z(O)^\bullet/H190(H)^+/P_{680}]_{initial}$ is predicted to involve unfavorable potentials, but could perhaps occur transiently. It is more likely that the $[Y_Z^{ox}/P_{680}]_{initial}$ state formed during the ns phase of P_{680}^+ reduction corresponds to a $[Y_Z(O)^\bullet/H190/B(H)^+/P_{680}]$ configuration, where B represents secondary proton acceptor(s) residing in a hydrogen-bonding network. For the final state, $[Y_Z^{ox}/P_{680}]_{final}$, the H/D isotope effects on the μs phases may reflect subsequent proton transfers through this network that further lower the potential of $Y_Z^\bullet$, as shown in Fig. 5B or C. This analysis predicts that these proton migrations must occur to allow complete reduction of P_{680}^+.

Both Shilstra et al. [75] and Renger and coworkers [76–78] favor a continuous relaxation within PSII on the ns to μs time scale that may, as noted above, reflect proton transfer through hydrogen-bonded networks in the complex. An alternate possibility arises from the fact that proton motion in such networks is generally fast and that the slow step in proton migration to bulk usually occurs at the aqueous interface (see below). If this is the case in PSII, then multiphasic P_{680}^+ reduction may reflect a situation in which some centers are optimally hydrogen bonded for proton migration to produce the final state above on the ns time scale. Other PSII centers, however, may have defects in their proton connectivity to bulk. The equilibration of these networks will be determined by relatively slow surface protonation/deprotonation events and thus may give rise to the μs components in P_{680}^+ reduction. In this view, distributed or stretched exponential kinetics, as have been observed in several other systems (e.g. [89]), provides a better description of the reduction of the primary donor by Y_Z. Whether multiphasic P_{680}^+ reduction reflects homogeneous or heterogeneous relaxation processes, awaits further experimental work.

2.2.4. Oxidation of Y_Z in apo-PSII

Y_Z reduces P_{680}^+ on the μs time scale with a pronounced pH dependence in PSII samples depleted of the Mn, Ca^{2+}, and Cl^- cofactors [40,90]. The oxidation of Y_Z in apo-PSII occurs with a halftime of ~20–30 μs at pH 5.0, which is three orders of magnitude slower than the fastest oxidation phases in the fully active enzyme (Table 3). If we assume that ρ remains unaltered in apo-PSII relative to active samples, the change in the Y_Z oxidation rate can arise from an increase in the Y_Z–P_{680}^+ distance or in the reorganization energy associated with the electron-transfer reaction. Alternatively, the measured rate is limited by processes other than electron tunneling. We discuss these three possibilities below.

We can use Eq. 4 to estimate the change in Y_Z–P_{680} distance necessary to decrease the rate of Y_Z oxidation from the ns to the μs time domain upon removal of the $(Mn)_4$ cluster. With $\lambda = 0.70$ eV and $\rho = 0.70$, as in O_2-evolving samples, and $\Delta G = -75$

meV, as measured for apo-PSII samples at pH 5.0 (Table 1), the electron tunneling rate is calculated to be 20 μs, when the Y_Z–P^+_{680} distance is increased from 9.5 to 14.1 Å. Such a distance change in PSII upon removal of Mn is unlikely, however, as this requires a significant rearrangement of the membrane-spanning helices of the PSII core. No data have been reported that support such a large-scale conformation change in the interior of PSII when Mn is released.

In a similar fashion, Eq. 4 can be used to predict the increase in λ needed to decrease the electron-transfer rate three orders of magnitude. If we assume a ρ of 0.70, a distance of 9.5 Å, and a ΔG of −75 meV, an electron tunneling rate of 20 μs requires that $\lambda = 1.66$ eV. This value is fairly high, considering that both P_{680} and Y_Z are located within a protein. Nonetheless, measurements on activation energies are consistent with an increase in λ in apo-PSII relative to oxygen-evolving samples. The E_A value for Y_Z oxidation is increased from 0.10 eV in the active enzyme [72] to 0.28–0.48 eV in apo-PSII, depending on the sample conditions (Table 3; [40,83,91]). With Eq. 5, this activation energy range corresponds to $\lambda = 1.32$–2.12 eV. Thus, reorganization energy effects are likely to contribute to the retardation in P^+_{680} reduction rate in apo-PSII.

The increased λ and E_A values most likely arise from increased water content in the Y_Z site in the absence of the $(Mn)_4$ cluster. The variation in the stability of Y_Z is consistent with the idea that water invades the active site in apo-PSII. Thus, $Y^\bullet_Z$ in both active samples and in preparations specifically depleted of Ca^{2+} is unaffected by the addition of external reductants [92,93]. In contrast, $Y^\bullet_Z$ is reduced on the ms time scale in apo-PSII and, upon addition of external reductants, decays with second order rate constants on the order of 10^5–10^7 M^{-1} s^{-1}, depending on the identity of the exogenous reductant [94–97]. These observations indicate that rapid access to the Y_Z site from bulk phase by a diffusional process, which implies increased solvent access, is only possible in the absence of the $(Mn)_4$ cluster; the OEC itself is considerably more protected.

The kinetic data are consistent with EMR studies that have been performed to quantify the number of exchangeable protons in the Y_Z site as a function of the integrity of the metal cluster [57,98,99]. The transient $Y^\bullet_Z$ radical can be cryotrapped for low-temperature studies in apo-PSII. In inhibited, but Mn-containing samples, there are a variety of treatments that lock PSII in a paramagnetic $S_2Y^\bullet_Z$ state that can be investigated by EMR spectroscopies. ESEEM spectra for $S_2Y^\bullet_Z$ suggest that two and two-four exchangeable protons are present in the $(Mn)_4Y_Z$ site in Ca-depleted [99] and acetate-treated [24,57,100] PSII samples, respectively. In apo-PSII, at least four exchangeable protons appear within hydrogen-bonding distance of the radical [99]. Similar conclusions were reached from a study on $Y^\bullet_Z$ in metal-depleted samples from *Synechocystis* [57]. Thus, the magnetic-resonance work indicates that the number of exchangeable protons in the close vicinity of Y_Z increases when the metal cluster is removed. These results, which imply a significant solvent access in apo-PSII, are consistent with the requirements for the assembly of the holo-enzyme (see [101] and references therein), as Mn^{2+}, Ca^{2+}, and Cl^- must have fast access to their binding sites near Y_Z.

A third explanation for the slow oxidation rate of Y_Z in apo-PSII is that this process is limited by reactions other than electron tunneling. H/D isotope measurements on the rate of the $Y_Z \rightarrow P^+_{680}$ electron transfer suggest that proton-linked events limit this reaction in the apo system. An H/D isotope effect of 2.5–2.7 has been reported for apo-PSII prepared from plants [40,83]. Diner et al. studied the H/D isotope effect on Y_Z oxidation as a function of pH in *Synechocystis* apo-PSII and found a maximum of 3.64 at pH 7.0 [57]. Debus and coworkers found H/D isotope effects of 1.7–2.6, depending on the kinetic phase, at all pH values [60]. These isotope effects suggest that hydrogen bonding to Y_Z is perturbed from an optimal geometry in apo-PSII (see Fig. 6D), which slows electron transfer to P^+_{680}.

To summarize, the slow oxidation of Y_Z in apo-PSII is likely to arise from an increase in λ that may result from an increase in the solvent accessibility to the site and/or perturbations to the hydrogen-bonding geometry in the Y_Z/H190 site. Returning to the active enzyme, these considerations suggest that a well-tuned interaction between Y_Z and H190, and perhaps additional base(s) as well, is essential to make the tyrosine kinetically competent to reduce P^+_{680} sufficiently quickly to ensure a high quantum yield in the primary charge separation in PSII.

2.2.5. Oxidation of Y_Z in Ca^{2+} and Cl^--depleted PSII

The oxidation of Y_Z occurs on the μs time scale in samples that are treated with acetate [102] or specifically depleted of Ca^{2+} [103]. In contrast, Y_Z is oxidized with ns kinetics in Cl-depleted PSII samples [103–105]. The rates of Y_Z oxidation in these inhibited samples are summarized in Table 3. As discussed above, the Y_Z site appears to be more ordered in acetate-treated and Ca-depleted samples relative to apo-PSII. This suggests that the slow oxidation rates, Y_Z/H190, observed in acetate-treated or Ca-depleted PSII arise from a perturbation in the hydrogen bonding of the site. For Cl-depleted PSII, the integrity of the Y_Z site appears to be less perturbed; the Y_Z-H190 interaction is likely to be intact, but the interactions between $Y_Z^{\bullet}$ and the substrate bound to the $(Mn)_4$ cluster is apparently altered significantly.

2.3. The proton and electron currents at Y_Z

The third critical function of Y_Z is to interface the pure electron-transfer chemistry that occurs between the P_{680}/Q_A couple during primary charge separation to the proton-coupled, water-oxidation chemistry. The discussion thus far has summarized data that indicate that Y_Z occurs as the protonated, neutral tyrosine in the active system and that this species is converted to the deprotonated, neutral radical during the reduction of P_{680}^+. Thus, oxidation of Y_Z involves pcet and is the first step in the water-oxidizing process during which protons are mobilized. The thermodynamic considerations above indicate that the proton released during the oxidation of the tyrosine by P_{680}^+ must be liberated to the aqueous phase, rather than retained in the protein matrix, in order for the redox chemistry to proceed efficiently. The μs kinetic phases observed during P_{680}^+ reduction are consistent with this idea, as they are likely to reflect the progressive lowering of the $Y_Z^{\bullet}$ potential, and its correspondingly increased effectiveness as a donor to P_{680}^+, during proton migration to the lumen. Whether proton release to bulk occurs upon Y_Z oxidation, however, has been a point of contention and considerable effort has gone into resolving this issue. The primary counter indicators to $Y_Z/Y_Z^{\bullet}$-linked domino deprotonation to the lumen have been data on the chlorophyll bandshifts that accompany Y_Z redox change and the characteristics of the proton release

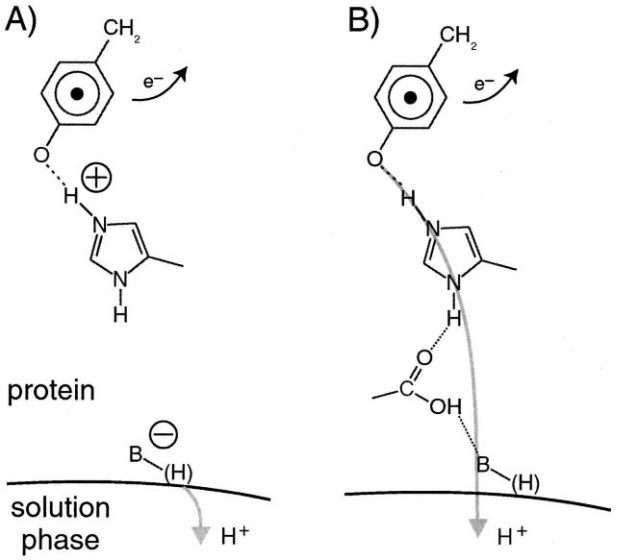

Fig. 7. Schematic representation of two mechanisms for proton release upon oxidation of Y_Z. In (A), an electrostatic mechanism for proton release to the solution phase is shown; in (B), direct, domino proton release through a hydrogen-bonded network is presented.

observed during water oxidation. In the sections below, we review this situation and then turn to a consideration of the mechanism by which $Y_Z^{\bullet}$ is reduced.

2.3.1. Electrostatic versus hydrogen-bonded network proton release upon Y_Z oxidation

Junge and his coworkers have shown in a series of careful and definitive measurements that protons are released on the same time scale as Y_Z is oxidized in various PSII preparations [106,107]. Two interpretations have been advanced for this observation, as illustrated in Fig. 7. In the first model, the observed proton release is electrostatic (Fig. 7A; [41,43]). Oxidation of Y_Z liberates a proton that is locally trapped, the resulting positive charge shifts the pK_a's of remote bases electrostatically, and these release protons in response. As $Y_Z^{\bullet}$ is reduced, the locally trapped proton 'rocks' back to the phenol oxygen to regenerate the protonated, neutral tyrosine. In this view, the increased potential available at $Y_Z^{\bullet}$ as the result of the trapped charge provides an electrostatic promotion to the potential of the $(Mn)_4Y_Z^{\bullet}$ cluster that is necessary for water oxidation [40,108]. In the second scenario (Fig. 7B), the appearance of protons in the bulk phase is taken to reflect domino deprotonation through a hydrogen-

bonded network that includes H190 and E189, additional amino acids, and water molecules intercalated into the protein matrix. In this model, protons are sloughed through the network to allow Y_Z to act as an effective electron donor to P^+_{680}, as discussed above, and then as an abstractor of hydrogen atoms from manganese-bound water and hydroxide as the S cycle clocks through its states [3,7,20,28,109].

Experiments and arguments aimed at distinguishing between these two models have relied on several lines of inquiry. These include the bandshifts that are observed in pigment absorption spectra on the time scale of Y_Z redox chemistry, the rate of proton release, the pH-dependence of this rate, and the pattern of proton release during water oxidation in various preparations. During the Y_Z redox cycle, characteristic perturbations in both the blue and red spectral regions have been interpreted to reflect the creation of uncompensated charge as Y_Z is oxidized [41,43, 59,65]. As discussed in more detail elsewhere [66], this interpretation is just one of several that can account for the observed spectral shifts. For example, dipole rearrangements or changes in hydrogen-bond strength, without the creation of uncompensated charge, may accompany Y_Z oxidation and produce the observed spectral perturbations. In myoglobin, for example, electrostatic effects in the distal pocket of the heme have pronounced effects on the stretching frequencies observed for bound carbon monoxide [110] and in rubredoxin, a shift in an α-helix of about 0.4 Å changes the potential of the iron redox center by approximately 50 mV [111]. Similar dipole and structural pertubations may be in effect in PSII and these must be considered before the observed pigment bandshifts can be taken as unequivocal evidence for charge creation as Y_Z is oxidized.

The kinetics of the proton release have been used as a second means by which to invoke electrostatic release. Electrostatic release is often taken to be a rapid event that is limited only by the pK_a of the releasing group [41,43], although conformational effects are sometimes invoked in retarding the process [32]. By contrast, proton migration through protein has been portrayed as a slower process that is unable to account for the rapid, 10 μs proton-release kinetics that can be observed. This criticism, however, is not particularly strong. A variety of experiments in both natural and model systems has shown that proton migration through a protein matrix is quite rapid, easily on the μs time scale, and that the rate-limiting step usually involves the deprotonation step at the protein/water interface [112,113], as depicted in Fig. 8. Thus, resolution of this issue is unlikely to come from kinetic arguments, as both electrostatic and domino deprotonation can occur sufficiently rapid to account for the observed data.

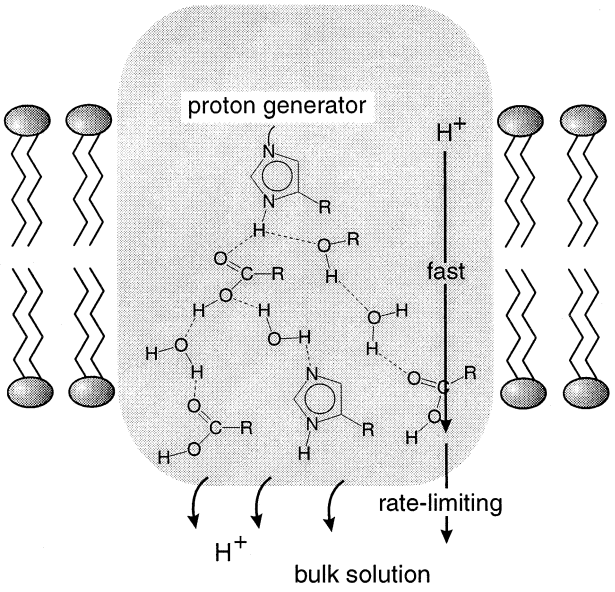

Fig. 8. Characteristics of proton movement through hydrogen-bonded networks and release at the protein/bulk solution interface. In general, proton motion in the protein is facile and the overall proton release is limited by the kinetics of interfacial release (see, for example, [112–115]).

The observation of an increase in the rate of the proton release as the pH is lowered in the buffer solution has been used as a third argument for an electrostatic origin of the fast proton release [107]. This is based on the prediction that the rate of interfacial proton release is expected to increase as the pK_a of the releasing group decreases [113]. But, the rate of proton conduction through a hydrogen-bonded chain has also been observed to increase at lower pH [114,115]. Thus, measurements of the pH dependence of the proton-release kinetics can not distinguish between the two models in Fig. 7, since the two proton-release mechanisms can have similar pH profiles.

Finally, the extent of proton release as a function of S-state transition varies substantially with preparation and this has also been taken as an indicator of

uncompensated charge creation in the OEC [41,43]. In general, less well-resolved PSII preparations give more complex proton-release patterns. As ancillary polypeptides are stripped from the PSII core, this complexity is relieved and, in PSII core preparations, a pH-independent, 1:1:1:1 proton-release pattern accompanies the S-state transitions. This observation has been rationalized as reflecting increased exposure of acid/base groups, as the polypeptide composition of PSII is simplified [41,43]. This argument, however, seems counterintuitive, as dielectric screening should increase, not decrease, as the distance between the OEC and the bulk phase is reduced by biochemical resolution of the system. Recent work by Lavergne on the photosynthetic bacterial reaction center supports the intuition that increased solvent screening accompanies biochemical refinement [116]. In chromatophores, it appears that protonation of Q_B^- to produce the neutral semiquinone, $Q_BH^\bullet$, occurs, whereas in more biochemically resolved, reaction-center preparations, Q_B^- formation provokes substoichiometric proton uptake into the proton matrix without direct protonation of the anionic semiquinone. If similar effects are at play in PSII and uncompensated charge is created, one would expect to see maximal variation in proton release in the most resolved preparations; uncompensated charge at either $Y_Z^\bullet$ or the $(Mn)_4$ cluster should be stabilized in PSII core preparations. Instead, a consistent and stoichiometric pattern of proton release is observed in both oxygen-evolving and apo-PSII preparations. This argues that the proton release observed is inherent to the chemistry and thermodynamics of the system and that Y_Z necessarily deprotonates to bulk during its oxidation.

2.3.2. The proton chemistry during $Y_Z^\bullet$ reduction

The realization that $Y_Z^\bullet$ may act as a hydrogen-atom abstractor and be reduced by pcet during the S-state advances rationalizes important aspects of this process. In Krishtalik's thoughtful analysis of the water-oxidizing process, he postulated that the S-state transitions could only be kinetically competent if they are linked to the protonation of basic groups in the OEC that are created as the $S_n/Y_Z/P_{680}$ chemistry unfolds [37]. The $Y_Z^\bullet/Y_Z$ couple is ideal in this role, as the neutral tyrosine radical is generated during the reduction of P_{680}^+ on each S-state transition. Moreover, the pK_{red} of Y_Z is sufficiently high to drive each of the $S_n \rightarrow S_{n+1}$ processes [7]. Thus, if Y_Z deprotonates to bulk as it is oxidized, a single acid/base group meets the Krishtalik requirement for all four S-state transitions. A second important mechanistic aspect of water oxidation that is resolved by invoking $Y_Z^\bullet$ as a hydrogen-atom abstractor is the requirement that the potentials for each of the four redox transitions be similar, that is, that redox leveling occurs for the four, one-electron steps involved in producing O_2 from H_2O (see Fig. 3). Pecoraro has shown that this can occur in a multinuclear manganese complex, if each redox advance is electroneutral [117]. This point has been reinforced by recent work from Girerd's laboratory ([118]; see also [119]). The electroneutral, proton-coupled reduction of $Y_Z^\bullet$ satisfies this requirement. The fact that the O-H bond dissociation energies for manganese-bound water and hydroxide are similar [120–123], and only slightly less than that of the O-H bond in tyrosine [124], is quantitatively consistent with the requirement that redox leveling occurs for the $S_n \rightarrow S_{n+1}$ transitions.

Recent models for the chemistry that occurs in the OEC recognize the usefulness of coupling proton and electron transfer to $Y_Z^\bullet$ reduction. In several of these proposals, $Y_Z^\bullet$ is invoked as a hydrogen-atom abstractor, either by a sequential or concerted mechanism, on all [7,28,109,125] or some [3,20,108,126,127] of the S-state transitions. In the latter models, a molecular means by which to toggle the $Y_Z^\bullet/Y_Z$ couple between a pure electron-transfer function and a coupled electron/proton-transfer function as the S state clock proceeds is necessary. Owing to the short tunneling distance for protons (< 1 Å at rates pertinent to water splitting), it may be possible to accomplish this by using a fairly minor, S-state dependent, rearrangement of protein main or side chains. The uncompensated positive charge created by frustrated proton release on the pure electron-transfer steps, however, will feed back electrostatically on the redox cofactors and alter their energetics, as described above. It appears that only the $S_0 \rightarrow S_1$ transition, for which the difference in S_0/S_1 and S_1/S_2 potentials is ~ 300 mV, meets the criteria established by Pecoraro and Girerd (see above; [117,118]), and can proceed with net charge accumulation. These issues and their molecular implementa-

tion are likely to generate significant research activity in the near future.

A good understanding of the phenomenology of the $S_n \rightarrow S_{n+1}$ transitions is available. Thus, the kinetics of the individual S-state advances have been resolved, the deuterium isotope effects on each of these steps have been measured, and the temperature dependencies of these processes have been studied (for summaries, see [66,128]). Moreover, the effects of various biochemical treatments on the rates of $Y_Z^{\bullet}$ reduction have been characterized ([103,129–131]; K. Westphal, G.T. Babcock, in preparation). Briefly, these data show that the S-state transitions occur on the 10's of μs to 1 ms time scale in thylakoid and BBY preparations, depending on S state, and that they are not very sensitive to pH. Various biochemical perturbations to PSII slow the rates of these reactions, with the $S_3 \rightarrow S_4 \rightarrow S_0 + O_2$ transition being most susceptible. Deuterium isotope effects are small; k_H/k_D is less than 3 for any of the transitions. The activation energies are remarkably low and range from about 65 to 420 meV, with the $S_2 \rightarrow S_3$ transition being the most highly activated. If we assume an edge-to-edge distance between Y_Z and the $(Mn)_4$ cluster of less than 8 Å, consistent with recent distance estimates from magnetic-resonance work [22–26], then reasonable estimates of the driving force and of the reorganization energy lead to predictions of rates on the order of ps to ns, if the non-adiabatic treatment developed by Dutton, Moser and their coworkers is used. Conversely, if we assume a $(Mn)_4$–Y_Z distance of 8 Å, a driving force of 60 mV, and a protein packing factor of 0.75 (see above), we find that the reduction of $Y_Z^{\bullet}$ proceeds with a half-time of 30 μs only if an unrealistically high value of λ of 2 V is used.

The fact that a non-adiabatic treatment cannot rationalize the rates of the $S_nY_Z^{\bullet} \rightarrow S_{n+1}Y_Z$ reactions indicates that they are rate limited by other processes than electron tunneling or that they proceed adiabatically, that is, with strong coupling between the reactant and product states. This behavior is characteristic of radical-mediated, hydrogen-atom transfer processes [132–136]. For example, the linear free-energy relationships that describe the driving force dependence of the rates of hydrogen-atom abstraction by phenoxy radicals from O-H bonds in alcohols and peroxides [135] accurately correlate the rates of the S-state advances with the $S_nY_Z^{\bullet} \rightarrow S_{n+1}Y_Z$ equilibrium constants [7]. Ingold and his coworkers have studied the temperature dependence of hydrogen-atom abstraction by phenoxy radicals and find that the activation energies, like those for the S-state transitions, are quite low [136]. Moreover, because little charge develops during the atom transfer, outer sphere reorganizations are likely to be small and not especially sensitive to environmental perturbations. These considerations suggest that the rich literature available on organic radical reactions [132–136], and that being developed for the analogous inorganic processes, especially by Mayer's group [120,137], will be useful in understanding mechanistic aspects of the $S_nY_Z^{\bullet}$ chemistry. Taken together, the characteristics of the S-state advances indicate that more than simple electron transfer is involved. The coupling of proton and electron coordinates appears to be substantial in determining the properties of these reactions.

3. Conclusions

The role of Y_Z in initiating proton involvement in the reactions that lead to photosynthetic water oxidation has been recognized only recently. The thermodynamic and kinetic implications of this function for the tyrosine are significant, but the extent to which they are in force in PSII is controversial. The analysis above shows that the fate of the proton released upon Y_Z oxidation has significant effects on the $Y_Z^{\bullet}/Y_Z$ reduction potential, as well as in determining the function of the radical in the ensuing S-state advances. Within the context of the driving force available from the reduction of P_{680}^{+}, the thermodynamic analysis indicates that proton release through a hydrogen-bonded network to bulk is most compatible with the redox properties of tyrosine. Moreover, the slow kinetic phases of P_{680}^{+} reduction, which have provoked considerable discussion, can be rationalized as reflecting the progressive lowering of the tyrosine potential as the proton migrates away from the $Y_Z^{\bullet}$ site. The proton-coupled, electron transfer from Y_Z to P_{680}^{+} can be understood within the available theories for proton transfer and non-adiabatic electron transfer and a good understanding of which process is limiting

under various conditions in PSII has emerged. For the reduction of $Y_Z^{\bullet}$, on the other hand, a non-adiabatic treatment does not account for the rates and temperature dependencies of the $S_nY_Z^{\bullet} \rightarrow S_{n+1}Y_Z$ reactions, which indicates that other rate-limiting steps are involved. A more accurate description may require the incorporation of ideas that are available or are emerging from studies on radical-mediated, hydrogen-atom transfer processes. Finally, although spectroscopically and biochemically well characterized, the function and the chemical properties of the second redox-active tyrosine in PSII, Y_D, remain enigmatic.

4. Note added in proof

While this paper was under review, an article [J. Phys. Chem. A 1999, 103, 5989–5995] appeared by Dr. R.I. Cukier that deals with the theoretical aspects of dissociative proton-coupled electron transfer. This model provides good insight into the oxidation of Y_Z by P_{680}^{+} in both apo- and holo-PSII.

Acknowledgements

Support from a postdoctoral fellowship from the Swedish Foundation for International Cooperation in Research and Higher Education (C.T.) and from NIH Grant GM 37300 and the USDA Competitive Research Grants Office (G.T.B.) is gratefully acknowledged. The electrochemical data shown in Fig. 4 were obtained with support from NIH Grant GM 48130 (P. Leslie Dutton). We are indebted to Rick Debus for insightful comments about proton tunneling. We also thank Curt Hoganson, Fabrice Rappaport, Gernot Renger, Wolfgang Junge, Bruce Diner, Gary Brudvig, Vince Pecoraro, Colin Wraight, James Mayer, Margareta Blomberg, Per Siegbahn, Peter Brzezinski, Les Dutton, Chris Moser, and Chris Page for helpful discussions.

References

[1] K.-H. Rhee, E.P. Morris, J. Barber, W. Kühlbrandt, Nature 396 (1998) 283–286.
[2] R.J. Debus, Biochim. Biophys. Acta 1102 (1992) 269–352.
[3] R.D. Britt, in: D.R. Ort, C.F. Yocum (Eds.), Oxygenic Photosynthesis: The Light Reactions, Kluwer Academic Publishers, Dordrecht, 1996, pp. 137–164.
[4] J.H.A. Nugent, Eur. J. Biochem. 237 (1996) 519–531.
[5] V.K. Yachandra, K. Sauer, M.P. Klein, Chem. Rev. 96 (1996) 2927–2950.
[6] W. Rüttinger, G.C. Dismukes, Chem. Rev. 97 (1997) 1–24.
[7] C. Tommos, G.T. Babcock, Acc. Chem. Res. 31 (1998) 18–25.
[8] B.A. Diner, Methods Enzymol. 297 (1998) 337–360.
[9] C.F. Yocum, V.L. Pecoraro, Curr. Opin. Chem. Biol. 3 (1999) 182–187.
[10] C.W. Hoganson, G.T Babcock, in: H. Sigel, A. Sigel (Eds.), Metal Ions in Biological Systems, Vol. 37, Marcel Dekker, New York, 2000, p. 613–657.
[11] C.W. Hoganson, G.T. Babcock, Biochemistry 28 (1989) 1448–1454.
[12] B. Svensson, C. Etchebest, P. Tuffery, P. van Kan, J. Smith, S. Styring, Biochemistry 35 (1996) 14486–14502.
[13] B.A. Diner, P.J. Nixon, J.W. Farchaus, Curr. Opin. Struct. Biol. 1 (1991) 546–554.
[14] R.A. Roffey, D.M. Kramer, Govindjee, R.T. Sayre, Biochim. Biophys. Acta 1185 (1994) 257–270.
[15] H.-A. Chu, A.P. Nguyen, R.J. Debus, Biochemistry 34 (1995) 5839–5858.
[16] A.-M.A. Hays, I.R. Vassiliev, J.H. Golbeck, R.J. Debus, Biochemistry 37 (1998) 11352–11365.
[17] F. Mamedov, R.T. Sayre, S. Styring, Biochemistry 37 (1998) 14245–14256.
[18] A. Boussac, J.-L. Zimmermann, A.W. Rutherford, J. Lavergne, Nature 347 (1990) 303–306.
[19] B.J. Hallahan, J.H.A. Nugent, J.T. Warden, M.C.W. Evans, Biochemistry 31 (1992) 4562–4573.
[20] M.L. Gilchrist Jr., J.A. Ball, D.W. Randall, R.D. Britt, Proc. Natl. Acad. Sci. USA 92 (1995) 9545–9549.
[21] X.-S. Tang, D.W. Randall, D.A. Force, B.A. Diner, R.D. Britt, J. Am. Chem. Soc. 118 (1996) 7638–7639.
[22] D.J. MacLachlan, J.H.A. Nugent, J.T. Warden, M.C.W. Evans, Biochim. Biophys. Acta 1188 (1994) 325–334.
[23] K.V. Lakshmi, S.S. Eaton, G.R. Eaton, H.A. Frank, G.W. Brudvig, J. Phys. Chem. B 102 (1998) 8327–8335.
[24] P. Dorlet, M. Di Valentin, G.T. Babcock, J.L. McCracken, J. Phys. Chem. B 102 (1998) 8239–8247.
[25] J.M. Peloquin, K.A. Campbell, R.D. Britt, J. Am. Chem. Soc. 120 (1998) 6840–6841.
[26] K.V. Lakshmi, S.S. Eaton, G.R. Eaton, G.W. Brudvig, Biochemistry 38 (1999) 12758–12767.
[27] R.M. Cinco, J.H. Robblee, A. Rompel, C. Fernandez, V.K. Yachandra, K. Sauer, M.P. Klein, J. Phys. Chem. B 102 (1998) 8248–8256.
[28] G.T. Babcock, in: P. Mathis (Ed.), Photosynthesis: from Light to Biospere, Vol. II, Kluwer Academic Publishers, Dordrecht, 1995, pp. 209–215.
[29] L.N.M. Duysens, in: Photochemical Apparatus, Brookhaven Symposium in Biology No. 11, Brookhaven National Laboratory, Upton, NY, 1958, p. 18.

[30] R.T. Ross, M. Calvin, Biophys. J. 7 (1967) 595–614.
[31] V.V. Klimov, S.I. Allakhverdiev, S. Demeter, A.A. Krasnovskii, Dokl. Acad. Nauk. SSSR 249 (1979) 227–230.
[32] A.Y. Mulkidjanian, Biochim. Biophys. Acta 1410 (1999) 1–6.
[33] X. Lin, H.A. Murchison, V. Nagarajan, W.W. Parson, J.P. Allen, J.C. Williams, Proc. Natl. Acad. Sci. USA 91 (1994) 10265–10269.
[34] P. Juliot, G. Barbieri, R. Chabaud, Photochem. Photobiol. 10 (1969) 309–329.
[35] B. Kok, B. Forbuch, M. McGloin, Photochem. Photobiol. 11 (1970) 457–475.
[36] D.M. Kramer, C.A. Sacksteder, J.A. Cruz, Photosynth. Res. 60 (1999) 151–163.
[37] L.I. Krishtalik, Biochim. Biophys. Acta 849 (1986) 162–171.
[38] I. Vass, S. Styring, Biochemistry 30 (1991) 830–839.
[39] K. Brettel, E. Schlodder, H.T. Witt, Biochim. Biophys. Acta 766 (1984) 403–415.
[40] R. Ahlbrink, M. Haumann, D. Cherepanov, O. Bögershausen, A. Mulkidjanian, W. Junge, Biochemistry 37 (1998) 1131–1142.
[41] J. Lavergne, W. Junge, Photosynth. Res. 38 (1993) 279–296.
[42] H. Kretschmann, E. Schlodder, H.T. Witt, Biochim. Biophys. Acta 1274 (1996) 1–8.
[43] M. Haumann, W. Junge, in: D.R. Ort, C.F. Yocum (Eds.), Oxygenic Photosynthesis: The Light Reactions, Kluwer Academic Publishers, Dordrecht, 1996, pp. 165–192.
[44] J.G. Metz, P.J. Nixon, M. Rögner, G.W. Brudvig, B.A. Diner, Biochemistry 28 (1989) 6960–6969.
[45] C.A. Buser, L.K. Thompson, B.A. Diner, G.W. Brudvig, Biochemistry 29 (1990) 8977–8985.
[46] W.M. Clark, Oxidation-Reduction Potentials of Organic Systems, The Williams and Wilkins Company, Baltimore, VA, 1960.
[47] W.T. Dixon, D. Murphy, J. Chem. Soc. Faraday Trans. II 72 (1976) 1221–1230.
[48] P.R. Rich, B. Meunier, R. Mitchell, A.J. Moody, Biochim. Biophys. Acta 1275 (1996) 91–95.
[49] M.R.A. Blomberg, P.E.M. Siegbahn, G.T. Babcock, J. Am. Chem. Soc. 120 (1998) 8812–8824.
[50] C. Tommos, J.J. Skalicky, D.L. Pilloud, A.J. Wand, P.L. Dutton, Biochemistry 38 (1999) 9495–9507.
[51] F. Rappaport, J. Lavergne, Biochemistry 30 (1991) 10004–10012.
[52] M.Y. Okamura, G. Feher, Annu. Rev. Biochem. 61 (1992) 861–896.
[53] S. Un, X.-S. Tang, B.A. Diner, Biochemistry 35 (1996) 679–684.
[54] C. Tommos, X.-S. Tang, K. Warncke, C.W. Hoganson, S. Styring, J. McCracken, B.A. Diner, G.T. Babcock, J. Am. Chem. Soc. 117 (1995) 10325–10335.
[55] C. Berthomieu, R. Hienerwadel, A. Boussac, J. Breton, B.A. Diner, Biochemistry 37 (1998) 10547–10554.
[56] L.P. Candeias, S. Turconi, J.H.A. Nugent, Biochim. Biophys. Acta 1363 (1998) 1–5.
[57] B.A. Diner, D.A. Force, D.W. Randall, R.D. Britt, Biochemistry 37 (1998) 17931–17943.
[58] M. Haumann, A. Mulkidjanian, W. Junge, Biochemistry 38 (1999) 1258–1267.
[59] F. Rappaport, J. Lavergne, Biochemistry 36 (1997) 15294–15302.
[60] A.-M.A. Hays, I.R. Vassiliev, J.H. Golbeck, R.J. Debus, Biochemistry 38 (1999) 11851–11865.
[61] C. Tommos, L. Davidsson, B. Svensson, C. Madsen, W. Vermaas, S. Styring, Biochemistry 32 (1993) 5436–5441.
[62] X.-S. Tang, D.A. Chisholm, G.C. Dismukes, G.W. Brudvig, B.A. Diner, Biochemistry 32 (1993) 13742–13748.
[63] K.A. Campbell, J.M. Peloquin, B.A. Diner, X.-S. Tang, D.A. Chisholm, R.D. Britt, J. Am. Chem. Soc. 119 (1997) 4787–4788.
[64] R. Hienerwadel, A. Boussac, J. Breton, B.A. Diner, C. Berthomieu, Biochemistry 36 (1997) 14712–14723.
[65] B.A. Diner, X.-S. Tang, M. Zheng, G.C Dismukes, D.A. Force, D.W. Randall, R.D. Britt, in: P. Mathis (Ed.), Photosynthesis: from Light to Biospere, Vol. II, Kluwer Academic Publishers, Dordrecht, 1995, pp. 229–234.
[66] C. Tommos, C.W. Hoganson, M. Di Valentin, N. Lydakis-Simantiris, P. Dorlet, K. Westphal, H.-A. Chu, J. McCracken, G.T. Babcock, Curr. Opin. Chem. Biol. 2 (1998) 244–252.
[67] G.T. Babcock, R.E. Blankenship, K. Sauer, FEBS Lett. 61 (1976) 286–289.
[68] M. Boska, K. Sauer, W. Buttner, G.T. Babcock, Biochim. Biophys. Acta 772 (1983) 327–330.
[69] R.J. Debus, B.A. Barry, I. Sithole, G.T. Babcock, L. McIntosh, Biochemistry 27 (1988) 9071–9074.
[70] S. Gerken, K. Brettel, E. Schlodder, H.T. Witt, FEBS Lett. 237 (1988) 69–75.
[71] B. Meyer, E. Schlodder, J.P. Dekker, H.T. Witt, Biochim. Biophys. Acta 974 (1989) 36–43.
[72] H.-J. Eckert, G. Renger, FEBS Lett. 236 (1988) 425–431.
[73] E. Schlodder, K. Brettel, H.T. Witt, Biochim. Biophys. Acta 808 (1985) 123–131.
[74] P.B. Lukins, A. Post, P.J. Walker, A.W.D. Larkum, Photosynth. Res. 49 (1996) 209–221.
[75] M.J. Schilstra, F. Rappaport, J.H.A. Nugent, C.J. Barnett, D.R. Klug, Biochemistry 37 (1998) 3974–3981.
[76] G. Christen, F. Reifarth, G. Renger, FEBS Lett. 429 (1998) 49–52.
[77] G. Christen, G. Renger, Biochemistry 38 (1999) 2068–2077.
[78] G. Christen, A. Seeliger, G. Renger, Biochemistry 38 (1999) 6082–6092.
[79] M. Karge, K.-D. Irrgang, S. Sellin, R. Feinäugle, B. Liu, H.-J. Eckert, H.J. Eichler, G. Renger, FEBS Lett. 378 (1996) 140–144.
[80] M. Haumann, O. Bögershausen, D. Cherepanov, R. Ahlbrink, W. Junge, Photosynth. Res. 51 (1997) 193–208.
[81] C.C. Moser, J.M. Keske, K. Warncke, R.S. Farid, P.L. Dutton, Nature 355 (1992) 796–802.
[82] C.C. Page, C.C. Moser, X. Chen, P.L. Dutton, Nature 402 (1999) 47–52.

[83] G. Renger, G. Christen, M. Karge, H.-J. Eckert, K.-D. Irrgang, J. Biol. Inorg. Chem. 3 (1998) 360–366.
[84] P.J. O'Malley, J. Am. Chem. Soc. 120 (1998) 11732–11737.
[85] M.M. Szczesniak, S. Scheiner, J. Phys. Chem. 89 (1985) 1835–1840.
[86] S. Scheiner, Acc. Chem. Res. 27 (1994) 402–408.
[87] R.I. Cukier, D.G. Nocera, Annu. Rev. Phys. Chem. 49 (1998) 337–369.
[88] M.S. Graige, M.L. Paddock, J.M. Bruce, G. Feher, M.Y. Okamura, J. Am. Chem. Soc. 118 (1996) 9005–9016.
[89] S.J. Hagen, J. Hofrichter, W.A. Eaton, Science 269 (1995) 959–962.
[90] H. Conjeaud, P. Mathis, Biochim. Biophys. Acta 590 (1980) 353–359.
[91] S. Reinman, P. Mathis, Biochim. Biophys. Acta 635 (1981) 249–258.
[92] D.F. Ghanotakis, G.T. Babcock, C.F. Yocum, Biochim. Biophys. Acta 765 (1984) 388–398.
[93] N. Lydakis-Simantiris, P. Dorlet, D.F. Ghanotakis, G.T. Babcock, Biochemistry 37 (1998) 6427–6435; Errata, Biochemistry 37 (1998) 8816–8816.
[94] G.T. Babcock, K. Sauer, Biochim. Biophys. Acta 376 (1975) 329–344.
[95] C.T. Yerkes, G.T. Babcock, Biochim. Biophys. Acta 590 (1980) 360–372.
[96] D.F. Ghanotakis, C.T. Yerkes, G.T. Babcock, Biochim. Biophys. Acta 682 (1982) 21–31.
[97] G.T. Babcock, D.F. Ghanotakis, B. Ke, B.A. Diner, Biochim. Biophys. Acta 723 (1983) 276–286.
[98] G.T. Babcock, M. Espe, C. Hoganson, N. Lydakis-Simantiris, J. McCracken, W. Shi, S. Styring, C. Tommos, K. Warncke, Acta Chem. Scand. 51 (1997) 533–540.
[99] C. Tommos, J. McCracken, S. Styring, G.T. Babcock, J. Am. Chem. Soc. 120 (1998) 10441–10452.
[100] D.A. Force, D.W. Randall, R.D. Britt, Biochemistry 36 (1997) 12062–12070.
[101] G.M. Ananyev, G.C. Dismukes, Biochemistry 35 (1996) 14608–14617.
[102] Ö. Saygin, S. Gerken, B. Meyer, H.T. Witt, Photosynth. Res. 9 (1986) 71–78.
[103] A. Boussac, P. Sétif, A.W. Rutherford, Biochemistry 31 (1992) 1224–1234.
[104] T. Ono, H. Conjeaud, H. Gleiter, Y. Inoue, P. Mathis, FEBS Lett. 203 (1986) 215–219.
[105] M. Haumann, W. Drevenstedt, M. Hundelt, W. Junge, Biochim. Biophys. Acta 1273 (1996) 237–250.
[106] M. Haumann, W. Junge, Biochemistry 33 (1994) 864–872.
[107] O. Bögershausen, W. Junge, Biochim. Biophys. Acta 1230 (1995) 177–185.
[108] M. Haumann, W. Junge, Biochim. Biophys. Acta 1411 (1999) 86–91.
[109] C.W. Hoganson, G.T. Babcock, Science 277 (1997) 1953–1956.
[110] G.N. Phillips, M.L. Teodoro, T.S. Li, B. Smith, J.S. Olson, J. Phys. Chem. B 103 (1999) 8817–8829.
[111] P.D. Swartz, B.W. Beck, T. Ichiye, Biophys. J. 71 (1996) 2958–2969.
[112] M. Gutman, E. Nachliel, Biochim. Biophys. Acta 1015 (1990) 391–414.
[113] M. Gutman, E. Nachliel, Biochim. Biophys. Acta 1231 (1995) 123–138.
[114] P. Ädelroth, P. Brzezinski, B.G. Malmström, Biochemistry 34 (1995) 2844–2849.
[115] Y. Marantz, E. Nachliel, A. Aagaard, P. Brzezinski, M. Gutman, Proc. Natl. Acad. Sci. USA 95 (1998) 8590–8595.
[116] J. Lavergne, C. Matthews, N. Ginet, Biochemistry 38 (1999) 4542–4552.
[117] N.A. Law, M.T. Caudle, V.L. Pecoraro, Adv. Inorg. Chem. 46 (1999) 305–440.
[118] O. Horner, E. Anxolabehere-Mallart, M.-F. Charlot, L. Tchertanov, J. Guilhem, T.A. Mattioli, A. Boussac, J.-J. Girerd, Inorg. Chem. 38 (1999) 1222–1232.
[119] H.H. Thorp, J.E. Sarneski, G.W. Brudvig, R.H. Crabtree, J. Am. Chem. Soc. 111 (1989) 9249–9250.
[120] K.A. Gardner, J.M. Mayer, Science 269 (1995) 1849–1851.
[121] M.J. Baldwin, V.L. Pecoraro, J. Am. Chem. Soc. 118 (1996) 11325–11326.
[122] M.R.A. Blomberg, P.E.M. Siegbahn, S. Styring, G.T. Babcock, B. Åkermark, P. Korall, J. Am. Chem. Soc. 119 (1997) 8285–8292.
[123] M.T. Caudle, V.L. Pecoraro, J. Am. Chem. Soc. 119 (1997) 3415–3416.
[124] J. Lind, X. Shen, T.E. Eriksen, G. Merényi, J. Am. Chem. Soc. 112 (1990) 479–482.
[125] P.E.M. Siegbahn, R.H. Crabtree, J. Am. Chem. Soc. 121 (1999) 117–127.
[126] V.L. Pecoraro, M.J. Baldwin, M.T. Caudle, W.-Y. Hsieh, N.A. Law, Pure Appl. Chem. 70 (1998) 925–929.
[127] J. Limburg, V.A. Szalai, G.W. Brudvig, J. Chem. Soc. Dalton Trans. 9 (1999) 1353–1361.
[128] M. Karge, K.-D. Irrgang, G. Renger, Biochemistry 36 (1997) 8904–8913.
[129] M.R. Razeghifard, R.J. Pace, Biochim. Biophys. Acta 1322 (1997) 141–150.
[130] M.R. Razeghifard, T. Wydrzynski, R.J. Pace, R.L. Burnap, Biochemistry 36 (1997) 14474–14478.
[131] M. Hundelt, A.-M.A. Hays, R.J. Debus, W. Junge, Biochemistry 37 (1998) 14450–14456.
[132] S.S. Shaik, H.B. Schlegel, S. Wolfe, in: Theoretical Aspects of Physical Organic Chemistry: the S_N2 Mechanism, Wiley, New York, 1992.
[133] A. Pross, H. Yamataka, S. Nagase, J. Phys. Org. Chem. 4 (1991) 135–140.
[134] C. Alhambra, J.L. Gao, J.C. Corchado, J. Villa, D.G. Truhlar, J. Am. Chem. Soc. 121 (1999) 2253–2258.
[135] L.R. Mahoney, M.A. DaRooge, J. Am. Chem. Soc. 97 (1975) 4722–4731.
[136] M. Foti, K.U. Ingold, J. Lusztyk, J. Am. Chem. Soc. 116 (1994) 9440–9447.
[137] J.M. Mayer, Acc. Chem. Res. 31 (1998) 441–450.